Journal of Photochemistry & Photobiology, B: Biology 251 (2024) 112842

Contents lists available at ScienceDirect

Journal of Photochemistry & Photobiology, B: Biology

journal homepage: www.elsevier.com/locate/jphotobiol

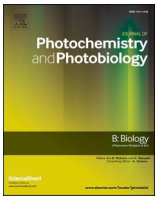

Evaluation of the cytotoxic and immunomodulatory effects of sonodynamic therapy in human pancreatic cancer spheroids

Federica Foglietta [a], Patrizia Panzanelli [b], Riccardo Pizzo [b], Marta Giacone [a], Carlo Della Pepa [a], Gianni Durando [c], Loredana Serpe [a,*], Roberto Canaparo [a]

[a] Department of Drug Science and Technology, University of Torino, Via Pietro Giuria 13, 10125 Torino, Italy
[b] Department of Neuroscience Rita Levi Montalcini, University of Torino, Via Cherasco 15, 10126 Torino, Italy
[c] National Institute of Metrological Research (INRIM), Strada delle Cacce 91, 10135 Torino, Italy

ARTICLE INFO

Keywords:
Sonodynamic therapy
Ultrasound
IR-780
Immunogenic cell death
cancer spheroids

ABSTRACT

Sonodynamic therapy (SDT) exploits the energy generated by ultrasound (US) to activate sound-sensitive drugs (sonosensitizers), leading to the generation of reactive oxygen species (ROS) and cancer cell death. Two-dimensional (2D) and three-dimensional (3D) cultures of human pancreatic cancer BxPC-3 cells were chosen as the models with which to investigate the therapeutic effects of the US-activated sonosensitizer IR-780 as pancreatic cancer is still one of the most lethal types of cancer. The effects of SDT, including ROS production, cancer cell death and immunogenic cell death (ICD), were extensively investigated. When subjected to US, IR-780 triggered significant ROS production and caused cancer cell death after 24 h ($p \leq 0.01$). Additionally, the activation of dendritic cells (DCs) led to an effective immune response against the cancer cells undergoing SDT-induced death. BxPC-3 spheroids were developed and studied extensively to validate the findings observed in 2D BxPC-3 cell cultures. An analysis of the pancreatic cancer spheroid section revealed significant SDT-induced cancer cell death after 48 h after the treatment ($p \leq 0.01$), with this being accompanied by the presence of SDT-induced damage-associated molecular patterns (DAMPs), such as calreticulin (CRT) and high mobility group box 1 (HMGB1). In conclusion, the data obtained demonstrates the anticancer efficacy of SDT and its immunomodulatory potential *via* action as an ICD-inducer.

1. Introduction

Pancreatic ductal adenocarcinoma (PDAC) has a lower survival rate than any other cancer [1,2], while progression in patient outcomes that has basically stood still for the past forty years [3]. PDAC is often diagnosed at advanced stages and the majority of patients (30–40%) present diffuse metastases, for which the median survival is just 5–9 months after diagnosis [4].Furthermore, most PDAC patients undergoing surgery harbour non-radiographically detectable micrometastases that are resistant to adjuvant chemotherapy [5]. PDAC is therefore a substantial on-going challenge for oncology with there being a burning need for novel and effective treatment options. Although apoptosis has long been considered a tolerogenic and non-immunogenic process, there exists increasing amounts of evidence to show that dying apoptotic cells can trigger an inflammatory response [6]. In fact, immunogenic cell death (ICD) is a keystone in cancer management as it elicits a massive antitumour immune response *via* the release of specific damage-associated molecular patterns (DAMPs), such as adenosine triphosphate (ATP), calreticulin (CRT), and high mobility group box protein B1 (HMGB1), which act as danger signals [7,8]. The interaction between DAMPs and specific receptors stimulates the recruitment and the activation of macrophages and dendritic cells (DCs), which promote immune-mediated elimination within the tumour microenvironment. ICD inducers are classified into Type I and Type II, according to whether they are able to induce endoplasmic reticulum (ER) stress indirectly (Type I, including several chemotherapeutics used on a low-dose regimen) [9], or directly (Type II, such as in hypericin-based photodynamic therapy) [10–12]. Sonodynamic therapy (SDT) can also be considered a potential ICD inducer as one of their common characteristics is that of inducing ER stress and reactive oxygen species (ROS)

* Corresponding author at: Department of Drug Science and Technology, University of Torino, Via Giuria 13, 10125 Torino, Italy.
E-mail addresses: federica.foglietta@unito.it (F. Foglietta), patrizia.panzanelli@unito.it (P. Panzanelli), riccardo.pizzo@unito.it (R. Pizzo), marta.giacone@edu.unito.it (M. Giacone), carlo.dellapepa@unito.it (C.D. Pepa), g.durando@inrim.it (G. Durando), loredana.serpe@unito.it (L. Serpe), roberto.canaparo@unito.it (R. Canaparo).

https://doi.org/10.1016/j.jphotobiol.2024.112842
Received 1 November 2023; Received in revised form 27 December 2023; Accepted 7 January 2024
Available online 10 January 2024

production. SDT exploits non-toxic sonosensitizers, ultrasound (US) and oxygen to activate a cascade of reactions that generates ROS, leading to massive cell death, making it a promising technique for the treatment of solid tumours [13,14]. SDT can be identified as an energy-driven cancer therapeutic modality that displays, as its main features, non-invasiveness, deep tissue-penetration capability, and time- and space-selective cancer cell killing [15,16]. Indeed, the high penetrative power of US allows deep-seated tumour regions to be precisely treated, minimizing damage to surroundings. Moreover, SDT is able to induce significantly stronger cytotoxic effects in cancer cells than in non-cancer cells, thus enhancing the safety of this approach. This cancer-cell-specific cytotoxicity has been ascribed to the greater plasma membrane fluidity of cancer cells, compared to that of normal cells, suggesting that cancer cells have lower stiffness resistance to US-mediated mechanical stress [17–19].

SDT has also shown the ability to reprogram anti-inflammatory and pro-tumoral M_2 tumour associated macrophages into pro-inflammatory and anti-tumour M_1 macrophages, further enhancing the immune response [20,21]. Li et al. have investigated the use of the sonosensitizer 2-[2-[2-Chloro-3-[(1,3-dihydro-3,3-dimethyl-1-propyl-2H-indol-2-ylidene)ethylidene]-1-cyclohexen-1-yl]ethenyl]-3,3-dimethyl-1-propylindolium iodide (IR-780), a lipophilic cationic near-infrared dye, against 4T1 breast cancer *in vitro* and *in vivo* [22], and observed marked tumour-growth inhibition. Moreover, IR-780 exhibits high fluorescence intensity and remarkable photothermal conversion efficiency, making it both an excellent photothermal and imaging agent for *in vivo* tumour tracking. We hypothesize that the combined use of US and IR-780, used as a sonosensitizer, may synergistically reduce tumour burden and trigger a considerable immune response, thereby providing an alternative option for PDAC treatment and further strengthening anticancer approaches against PDAC. We describe, herein, a focused investigation into the US-mediated cytotoxicity of IR-780 against *in vitro* three-dimensional (3D) PDAC, which closely mirrors *in vivo* tumour cellular architecture and will therefore support translation to future animal studies [23,24].

2. Materials and Methods

2.1. 2D and 3D BxPC-3 Cell Cultures

The human pancreatic cancer cell line BxPC-3 was obtained from the American Type Culture Collection (cat n. 1687, ATCC, Milano, Italy). BxPC-3 cells were cultured as a two-dimensional (2D) monolayer in RPMI 1640 medium (cat n. L0500–500) enriched with 10% (*v*/v) foetal calf serum (cat n. 341,506), 2 mM L-glutamine (cat n. G7513), penicillin (100 units/mL, cat n. 1,502,701) and streptomycin (100 μg/mL, cat n. S9137) (Sigma-Aldrich, Milano, Italy). Growing monolayers were cultured at +37 °C in a humidified atmosphere with 5% of CO_2 in a dark incubator (Thermo Fisher Scientific, Milano, Italy) and passaged regularly at sub-confluence with 0.05% trypsin-0.02% EDTA solution (cat n. SCM090, Sigma-Aldrich, Milano, Italy). Cells were used for experiments in their first 12 passages from the first thawing. BxPC-3 cells were cultured as three-dimensional (3D) spheroids using the agarose-coating technique. Briefly, agarose (cat n. A0576, Sig-ma-Aldrich, Milano, Italy) was resuspended in phosphate buffered saline (PBS) at 1.5%, and then sterilized using autoclave sterilization cycles at 121 °C for 15 min. Agarose was then maintained in a hot water bath to avoid solidification, and 60 μL of solution was added into each well of 96-U well plates (cat n. 3474, BRAND GMBH + CO KG, Wertheim, Germany) for coating. The plates were left to cool for 15 min and stored for 24 h under dark conditions. To generate BxPC-3 spheroids, varying densities of cells (5×10^3, 8×10^3 and 12×10^3 cells/200 μL medium) were seeded on agarose-coated plates. Spheroid growth and conformation were monitored up to 6-days post seeding with a DMI4000B fluorescent microscope 10× (Leica Microsystems, Milano, Italy). A density of 5×10^3 cells did not lead to spherical conformation after 4, 5 and 6 days, whereas a density of 8×10^3 cells resulted in an unstable conformation after 4, 5 and 6 days. However, spheroids seeded at a density of 12×10^3 cells formed a stable mass, which progressively compacted after 4, 5 and 6 days. In accordance with these results, the cell density chosen for the consequent 3D experiments was 12×10^3 cells/200 μL medium.

2.2. Evaluation of IR-780 Cytotoxicity in 2D BxPC-3 Cell Cultures

IR-780 iodide (cat n. 425,311) was purchased from Sigma-Aldrich (Milano, Italy) and a mother stock solution of 10 mg/mL was dissolved in dimethyl sulfoxide (DMSO, cat n. D1435, Sigma-Aldrich, Milano, Italy) and then stored at −20 °C. To assess IR-780 cytotoxicity in BxPC-3 cells, 5×10^3 cells were seeded in 200 μL of culture medium at increasing IR-780 concentrations (0.01, 0.1, 1, 10 and 100 μg/mL) in 96-well culture plates (Corning, Milano, Italy) whit several replicates ($n = 5$) for each condition. Cell proliferation was examined at different time points (24, 48 and 72 h) using a WST-1 assay (cat n. 11,465,007,001, Roche-Applied, Milano, Italy) *via* the addition of 10 μL of WST-1 reagent to 100 μL of cell culture medium in each well of the cell culture plates and the subsequent incubation of the plates at +37 °C for 3 h. The absorbance of each well was determined at 450 and 620 nm (reference wavelength) using a microplate reader (Asys UV340, Biochrom, UK). IR-780 cytotoxicity is expressed as a percentage (%), according to the following equation: % cytotoxicity = (absorbance of untreated cells - absorbance of treated cells)/absorbance of untreated cells x 100. IR-780 IC_{50} (the drug inhibitory concentration needed to inhibit 50% of cell growth) was then calculated using CalcuSyn software, version 2.0 (Biosoft, Cambridge, UK).

2.3. Sonodynamic Treatment of 2D and 3D BxPC-3 Cell Cultures

A piezoelectric plane wave transducer (2.54 cm diameter) was used to generate the ultrasound (US) field. This system operates at a frequency of 1.505 MHz in conjunction with a power amplifier (Type AR 100A250A, Amplifier Research, Souderton, USA) and a function generator (Type 33,250, Agilent, USA). A custom-built mechanical adaptor was connected to the 1 cm diameter polystyrene tube containing either the cell suspension or spheroids. The adaptor guarantees high reproducibility when filled with ultrapure water. The *in vitro* sonodynamic therapy (SDT) experiments were performed under subdued light, and the temperature of the medium was also monitored to avoid hyperthermia during the experiment. BxPC-3 cells were exposed to different US parameters for experiments on 2D (1.505 MHz, 0.63 W/cm^2, continuous wave mode for 3 min) and 3D (1.505 MHz, 1.66 W/cm^2, 60% duty cycle for 3 min) cultures. Briefly, 2D cultured BxPC-3 cells at 80% confluence were detached with trypsin-0.02% ethylenediaminetetraacetic acid (EDTA) solution (Sigma-Aldrich, Milano, Italy), suspended in culture medium and normalized to 5×10^5 cells in 2.7 mL PBS polystyrene tubes before undergoing the following treatments: control (*i.e.*, untreated), US (1.505 MHz, 0.63 W/cm^2, continuous wave mode for 3 min), IR-780 (5 μg/mL pre-incubated for 24 h), and IR-780 + US. Following treatment, 2×10^3 cells were seeded in culture medium (100 μL) in replicates ($n = 5$) in 96-well culture plates. The WST-1 assay (Roche-Applied, Milano, Italy) was then carried out to evaluate the effect of the treatment on cell proliferation after 24, 48 and 72 h. For the 3D cell culture, 4 days after seeding, a total of 9 spheroids were selected per condition and placed in 2.7 mL PBS polystyrene tubes to undergo the following treatments: control (*i.e.*, untreated), US (1.505 MHz, 1.66 W/cm^2, 60% duty cycle for 3 min), IR-780 (20 μg/mL pre-incubated for 24 h), and IR-780 + US. Treatment efficacy was then evaluated after 48 h using optical microscopy imagines and flow cytometric analyses, as reported below.

2.4. Flow Cytometry

2.4.1. IR-780 Cell Uptake in 2D and 3D BxPC-3 Cell Cultures

The uptake of IR-780 by BxPC-3 2D monolayers was determined *via* the cytofluorimetric evaluation of the intracellular fluorescence of IR-780, carried out using an Accuri C6 flow cytometer (BD, Biosciences, Milano, Italy). 1.5×10^5 cells were seeded in a 6-well plate and then incubated with selected IR-780 concentrations (0.5 and 5 μg/mL) for 24 h. Following incubation, cells were washed with PBS, incubated with trypsin for 5 min at +37 °C and then processed in the flow cytometer (λ_{ex} 780 nm, λ_{em} 807–823 nm), logging 1×10^4 events at a medium flow rate and discarding cellular debris from the analysis. IR-780 fluorescence was expressed as the integrated mean fluorescence intensity (iMFI), *i.e.,* the product of the frequency of IR-780 positive cells and the mean fluorescence intensity of the cells. To evaluate IR-780 uptake by BxPC-3 cells grown as 3D cultures, spheroids were grown for 4 days in the incubator at 37 °C and, on day 4, 100 μL of the culture medium per well was replaced with medium that contained increasing concentrations of IR-780 (10, 20 and 30 μg/mL) for 24 h. When IR-780 incubation ended, 9 spheroids for each condition were transferred into a sterile tube, washed in 500 μL of PBS and incubated for 15 min with trypsin (500 μL) at 37 °C. After trypsin inactivation and cell-pellet centrifugation, cells that dissociated from the 3D structures were washed in PBS and subsequently analysed *via* flow cytometry, with 5×10^4 events at medium flow rate being considered and cellular debris being discarded from the analysis. IR-780 uptake in BxPC-3 cells was then evaluated according to the intracellular fluorescence of IR-780 (λ_{ex} 780 nm, λ_{em} 807–823 nm) and expressed as iMFI.

2.4.2. Cell Death Evaluation in 2D BxPC-3 Cell Cultures

Following SDT, BxPC-3 cell death was evaluated using the Dead Cell Apoptosis Kit with propidium iodide (PI) and Alexa Fluor® 488 annexin V for flow cytometry (cat n. V13245, Life Technologies, Milano, Italy), according to the manufacturer's instructions. Briefly, 5×10^5 BxPC-3 cells, previously incubated for 24 h with IR-780 (5 μg/mL) underwent US (0.63 W/cm^2, 1.505 MHz for 3 min), were seeded in culture flasks and incubated at 37 °C for 24 h. Following incubation, cells were exposed to trypsin for 5 min at +37 °C and collected in a sterile polystyrene tube. Cells were then stained with Alexa Fluor® 488-annexin V and PI for 15 min and the samples were then processed in the flow cytometer. A total of 1×10^4 events was used to measure PI (PI, λ_{ex} 535 nm, λ_{em} 617 nm) and Alexa Fluor® 488 annexin V (λ_{ex} 488 nm, λ_{em} 519 nm). Any cell debris with low forward light scatter (FSC) and side light scatter (SSC) were excluded from the analyses. Alexa Fluor® 488 annexin V and PI staining distinguishes early apoptotic (annexin V positive and PI negative) and late apoptotic or necrotic cells (annexin V and PI positive) from live cells (annexin V and PI negative). All analyses were performed using FCS Express software, version 4 (BD, Biosciences, Milano, Italy).

2.4.3. Evaluation of Immunogenic Cell Death-Related Damage Associated Molecular Patterns in 2D BxPC-3 Cell Cultures

For 2D cultures, calreticulin (CRT) exposure on the cell surface was investigated 1 and 6 h post-SDT and IR-780 treatment. Briefly, BxPC-3 cells were washed with PBS, incubated with trypsin for 5 min at +37 °C, and followed by incubation with 10 μg/mL of Alexa Fluor® 488 anti-CRT antibody (cat. n. ab196158, Abcam, Cambridge, UK) at room temperature (RT) for 40 min, under dark conditions. Following incubation, cells were washed twice with PBS and then analysed using a C6 flow cytometer (λ_{ex} 488 nm, λ_{em} 530 nm). High mobility group box 1 (HMGB1) occurrence was determined 24 h after treatment with SDT and IR-780. Briefly, BxPC-3 cells were washed with PBS, incubated with trypsin for 5 min at +37 °C and then with anti-HMGB1 antibody (cat. n. ab77302, Abcam, Cambridge, UK) (10 μg/mL) for 30 min at RT, under dark conditions. When incubation ended, cells were washed once with PBS and then incubated with the anti-mouse immunoglobulin G (whole molecule)-fluorescein isothiocyanate (FITC) antibody (1200; cat n. SAB4200738, Sig-ma-Aldrich, Milano, Italy) for 1 h at RT, covered from light. Finally, cells were washed twice with PBS at the end of incubation and then analysed using the C6 flow cytometer (λ_{ex} 488 nm, λ_{em} 530 nm). 1×10^4 events were considered in all the cytofluorimetric analyses with a medium flow rate, discarding cellular debris.

2.4.4. Evaluation of Reactive Oxygen Species Production

SDT-mediated intracellular ROS production was determined using CellROX™ green (cat n. C10492, Thermo Fisher Scientific, Rodano, Italy) for oxidative stress detection. Following treatment, BxPC-3 cells were incubated with 500 nM CellROX™ green at 37 °C for 30 min. Following CellROX™ green incubation, cells underwent washing with PBS, trypsinization and normalization to 5×10^5 in 2.7 mL of PBS, followed by US exposure. ROS production was determined *via* flow cytometry (λ_{ex} 488 nm and λ_{em} 530 nm) at different time points (*i.e.*, 1, 5, 15, 30, 60, 90 and 120 min) after US exposure; 1×10^4 events were considered and cell debris with low SSC and low FSC were excluded from the analyses. ROS production is expressed as iMFI ratio to highlight the ratiometric variation in fluorescence per time point compared to control cells (*i.e.*, untreated cells), while the iMFI ratio was calculated from the difference in the iMFI of treated and untreated cells over the iMFI of untreated cells [25].

2.5. Cell Death Evaluation in 3D BxPC-3 Cell Cultures

Forty-eight hours after treatment, cellular damage on the spheroid corona was investigated *via* PI staining (cat n. P4170, Sigma Aldrich, Milano, Italy). Briefly, spheroids were washed twice with PBS to eliminate excess medium, and then incubated with a solution of PI in PBS (100 μg/mL) for 20 min in the dark at RT. Following incubation, spheroids were washed twice with PBS to remove PI excess, and PI fluorescence images were then acquired (λ_{ex} 540 nm and λ_{em} 590 nm) using a Leica DMI4000B fluorescence microscope (Leica Microsystems, Milano, Italy). Images were then analysed using ImageJ software, version 2.0 (Fiji, Bristol, UK) to quantify the PI fluorescence of the BxPC-3 spheroids. The results are expressed as mean of PI intensity/μm^2 ± standard deviation.

2.6. Evaluation of Dendritic Cell Activation in Peripheral Blood Mononuclear Cells and SDT-Treated BxPC-3 Cell Co-Cultures

Peripheral blood mononuclear cells (PBMCs) obtained from a healthy volunteer were separated using a Ficoll-Paque (cat n. GE17–1440-02, Sigma-Aldrich, Milano, Italy) gradient. In order to isolate PBMCs, a 50 mL conical centrifuge tube was filled with 15 mL Ficoll and an equal volume of whole blood diluted with PBS (1:1) was layered on top. The tube was then centrifuged at 1400 rpm for 35 min at a low acceleration speed. The PBMCs present in the Ficoll and the plasma were gently collected *via* aspiration and placed in a 15 mL conical tube. Shortly afterwards, PBMCs were washed three times with 10 mL PBS and centrifuged at 1500 rpm for 10 min. PBMCs were then resuspended and maintained in PBS for cell count. PBMCs were co-cultured with BxPC-3 cells in complete RPMI-1640 medium in a 1:1 proportion for subsequent SDT experiments. Forty-eight hours prior to the co-culture, BxPC-3 cells were incubated with IR-780 (5 μg/mL) for 24 h and exposed to US (0.63 W/cm^2 at 1.505 MHz, continuous wave mode for 3 min). Immediately afterwards, 4×10^5 BxPC-3 cells treated with SDT and 4×10^5 PBMCs (1,1) were incubated for 1, 12 and 24 h at +37 °C in a humidified atmosphere containing 5% of CO_2 in a dark incubator. At the end of each time point, 10 μL/10^6 cells were incubated for 1 h with anti-CD83 antibody (cat n. CPA6468, Cohesion Bioscience, London, UK) to detect activated dendritic cells, and with anti-CD326 antibody (cat n. 326 A-100 T, Immunostep, Salamanca, Spain) to detect tumour cells. Cells were then washed with PBS to remove excess antibodies and data acquisition was carried out on a C6 flow cytometer,

considering 5×10^4 events at a medium flow rate and discarding cellular debris from the analysis. Flow cytometry data were then visualised and gated through FCS Express 4 software (BD, Biosciences, Milano, Italy) and the data are expressed as iMFI ratio to highlight the ratiometric variation in fluorescence per time point compared to untreated cells.

2.7. Evaluation of Immunogenic Cell Death-Related Damage Associated Molecular Patterns in BxPC-3 Spheroids

At the end of each treatment, 40 spheroids per condition were washed with PBS, fixed with paraformaldehyde 4% (cat n. 158,127, Sigma-Aldrich, Milano, Italy) at RT for 15 min, washed with PBS, finally embedded in Tissue-Tek® optimal cutting temperature (OCT) compound (Sakura Finetek, Staufen, Germany) and preserved at −20 °C prior to cryo-section. For the immunofluorescence staining of CRT, cryosections (15 μm) were incubated with 10 μg/mL of Alexa Fluor® 488 anti-CRT antibody (cat. ab196158, Abcam, Cambridge, UK) at RT for 40 min, covered form light. For the immunofluorescence staining of HMGB1, sections were incubated with 10 μg/mL of anti-HMGB1 antibody (cat. ab77302, Abcam, Cambridge, UK) at RT for 30 min, covered form light. Slides were then washed with PBS and incubated 1for 1 h at RT with anti-mouse immunoglobulin G (whole molecule)-FITC antibody (1:200; Sigma-Aldrich, Milano, Italy). In the last 10 min of incubation 4′,6-diamidino-2-phenylindole (DAPI, 1:100; cat n. 62,248, Thermo Fisher Scientific, Milan, Italy) was added to all slides. Sections were analysed *via* confocal microscopy (LSM 900, Zeiss, Milano, Italy), and images were captured at 20× magnification using ImageJ software, version 2.0 (Fiji, Bristol, UK).

2.8. Statistical Analysis

Data are presented as mean values ± standard deviation (SD) of three independent experiments. Prism software, version 9.2 (Graph-Pad, La Jolla, USA) was used to perform statistical analyses. According to the design of the experiment, *t*-test, one-way, two-way ANOVA and Bonferroni's test were used to calculate the threshold of significance, which was set at $p \leq 0.05$.

3. Results

3.1. Effect of Sonodynamic Treatment on 2D BxPC-3 Cell Cultures

Firstly, it was important to discover the optimal non-cytotoxic concentration of the sensitizer, *i.e.*, IR-780, prior to ultrasound (US) exposure for the subsequent sonodynamic therapy (SDT) experiments. BxPC-3 cells were then incubated with increasing concentrations of IR-780 and cytotoxicity was observed over a 72 h period. IR-780 showed slight cytotoxic activity at 10 μg/mL 24 h post-incubation (21.41% ± 6.87), whereas at the highest concentration tested, 100 μg/mL, IR-780 showed strong cytotoxicity over time (89.06% ± 1.57 at 24 h, 93.92% ± 0.89 at 48 h and 94.87% ± 0.30 at 72 h) (Fig. 1A). On the other hand, the lower concentrations of IR-780, 0.01, 0.1 and 1 μg/mL, did not demonstrate significant cytotoxicity in BxPC-3 cells at any time point (Fig. 1A). The data derived from cytotoxicity curves were used to calculate the half maximal inhibitory concentration (IC_{50}), which was calculated to be 50.25 ± 12.24 μg/mL at 24 h incubation, 26.30 ± 1.41 μg/mL at 48 h incubation and 25.6 ± 10.40 μg/mL at 72 h incubation (Fig. S1). Based on these results, the suitable IR-780 concentrations for subsequent SDT experiments were calculated to be 0.5 and 5 μg/mL, which correspond to the two-percentage inhibitory concentration (IC_{02}) and the fifteen-percentage inhibitory concentration (IC_{15}), respectively, following a 24 h incubation period. IR-780 uptake by BxPC-3 cells was then investigated by flow cytometry, using the fluorescent properties of the sonosensitizer, at these two concentrations. Since a statistically significant higher increase in IR-780 uptake was observed in BxPC-3 cells at the higher concentration of 5 μg/mL (Fig. 1B), it was decided

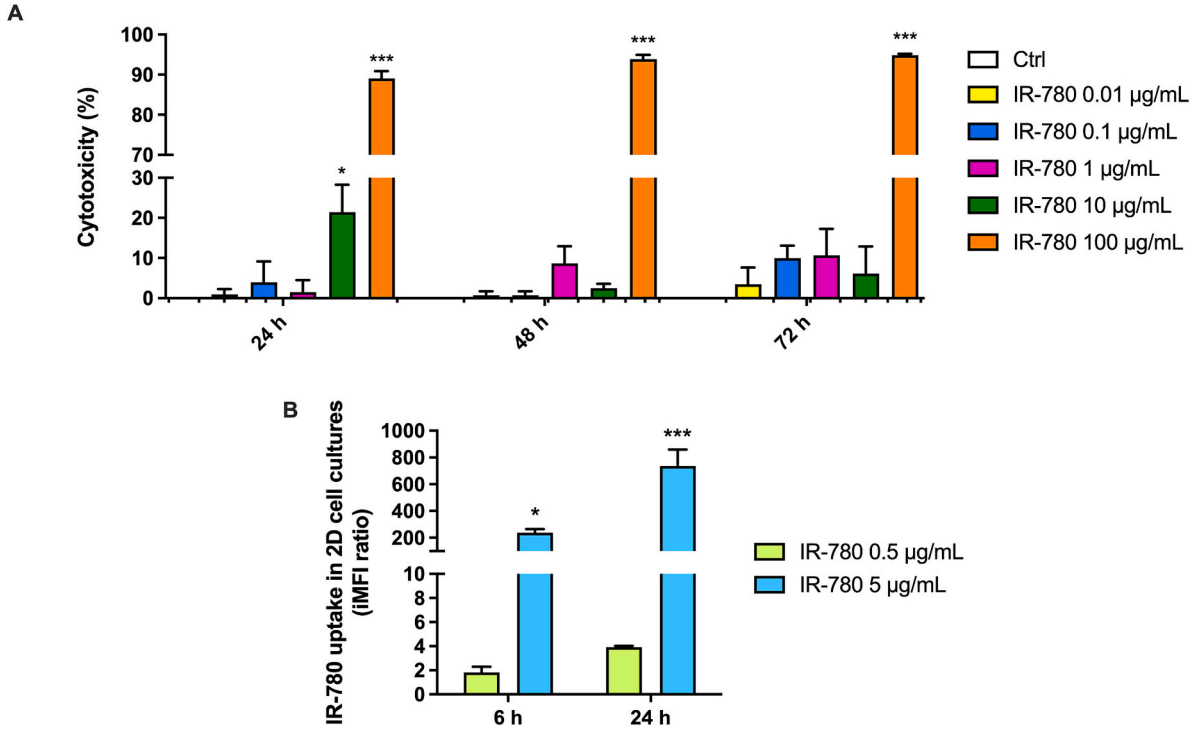

Fig. 1. IR-780 cytotoxicity in BxPC-3 cells and its cellular uptake. A) Cytotoxicity of BxPC-3 at increasing IR-780 concentrations (0.01, 0.1, 1, 10 and 100 μg/mL) were carried out *via* WST-1 assay after 24, 48 and 72 h of incubation and results are expressed as mean ± standard deviation (SD). Statistically significant difference *versus* untreated cells (Ctrl): * $p \leq 0.05$, *** $p \leq 0.001$. B) BxPC-3 cells were incubated with 0.5 and 5 μg/mL of IR-780 for 6 and 24 h, and cellular uptake was determined as integrated mean fluorescence intensity (iMFI) ratio values by flow cytometry and results are expressed as mean ± SD. Statistically significant difference between 0.5 μg/mL treated cells and 5 μg/mL treated cells: * $p \leq 0.05$, *** $p \leq 0.001$.

that this IR-780 concentration was to be employed for subsequent SDT experiments on two-dimensional (2D) BxPC-3 cell cultures.

3.2. Effects of SDT with IR-780 on Cell Proliferation, Cell Death and Reactive Oxygen Species (ROS) Production in 2D BxPC-3 Cell Cultures

BxPC-3 cell proliferation was investigated following treatment with IR-780 5 μg/mL, incubation for 24 h and US exposure (0.63 W/cm^2, 1.505 MHz, continuous wave mode for 3 min). As shown in Fig. 2A, a strong decrease in cell proliferation was detected when cells underwent SDT (IR-780 + US), starting from 24 h ($p \leq 0.05$) up to 72 h after treatment ($p \leq 0.01$). To further confirm the sonodynamic activation of IR-780, an evaluation of cell death was performed 24 h after SDT by flow cytometry (Fig. 2B and C). A significant increase in the percentage of late apoptotic cells (35.21% ± 0.65), compared to untreated cells (10.91% ± 0.71), was only visible when cells underwent SDT (IR-780 + US), while a significant decrease in the percentage of live cells (57.21% ± 1.47) was also observed compared to untreated cells (79.77% ± 0.93). ROS production is a pivotal step in the SDT mechanism of action [26], and SDT-mediated ROS production in BxPC-3 cells was therefore evaluated in a cytofluorimetric assay. Fig. 2D demonstrates that the exposure of IR-780 to US led to a statistically significant increase in ROS production, compared to untreated conditions, *i.e.,* Ctrl, from 1 min after the treatment ($p \leq 0.01$), followed by a slight reduction in ROS production that was sustained for up to 120 min ($p \leq 0.05$). These data underline IR-780's responsiveness to US and its suitability for use as a powerful sonosensitizer capable of exerting SDT-mediated selective anticancer cytotoxicity. Furthermore, in order to investigate SDT's particular selectivity towards cancer cells, an investigation of its effect on a non-cancer cell line was performed. A human dermal fibroblast cell line, HDF, was used for this purpose (for detailed information, see the Supporting Information). Firstly, lower IR-780 uptake was observed in HDF cells than in BxPC-3 cells at the same sensitizer concentration (Fig. S2), and, secondly, no cytotoxicity was observed in HDF cells after SDT (IR-780 and US) (Fig. S3). These data support the differences in responsiveness to SDT by cancer and non-cancer cells, as has also been described by other authors [17–19].

3.3. Induction of Immunogenic Cell Death-Related Damage Associated Molecular Patterns by SDT on 2D BxPC-3 Cell Cultures

Calreticulin (CRT) is an important ICD-related DAMP that functions mainly as an early "eat-me signal" produced during the ICD process [27]. CRT exposure on the cell surface was investigated 1 h and 6 h after SDT with IR-780 on BxPC-3 cells. As shown in Fig. 3, exposure of IR-780 to US induced a significant increase in CRT fluorescence compared to untreated cells (Ctrl), indicated by the dashed line, 6 h after treatment ($p \leq 0.05$). Moreover, the occurrence of HMGB1 (a late ICD-related DAMP), another hallmark of ICD that is released from the nucleus in the late stage sof cell death, [28] was investigated 24 h after treatment. Fig. 3 demonstrates that a significant increase in HMGB1 release, compared to untreated condition, *i.e.,* Ctrl, was detected after SDT with IR-780 ($p \leq 0.05$).

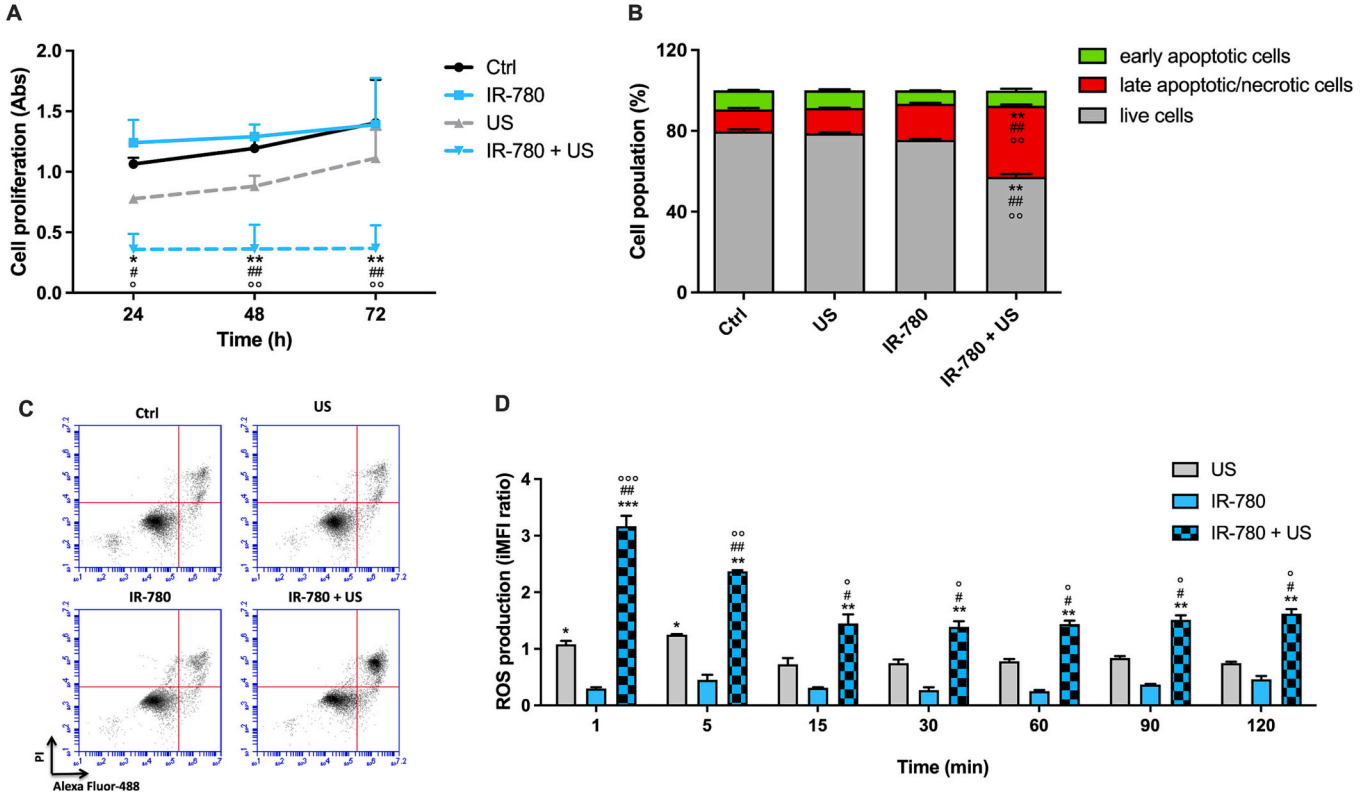

Fig. 2. Effect of IR-780 sonodynamic activity on BxPC-3 two-dimensional cell cultures. BxPC-3 cells were incubated for 24 h with IR-780 (5 μg/mL) and subsequently exposed to US (0.63 W/cm^2, 1.505 MHz, continuous wave mode for 3 min). A) Cell proliferation was measured at 24, 48 and 72 h after treatment by WST-1 assay and results are expressed as absorbance mean ± standard deviation (SD). B) Cell death induced by sonodynamic therapy (SDT, IR-780 + US) was determined by flow cytometry after 24 h and results are expressed as cell percentage mean ± SD. C) Representative cytofluorimetric dot plots of cell death. D) The production of reactive oxygen species (ROS) in BxPC-3 cells was determined by flow cytometry up to 120 min from treatments as integrated mean fluorescence intensity (iMFI) ratio and results are expressed as mean ± SD. Statistically significant difference *versus* untreated cells (Ctrl): * $p \leq 0.05$, ** $p \leq 0.01$, *** $p \leq 0.001$; statistically significant difference between IR-780 + US and IR-780: $^{\#}$ $p \leq 0.05$, $^{\#\#}$ $p \leq 0.01$ and statistically significant difference between IR-780 + US and US: $^{\circ}$ $p \leq 0.05$, $^{\circ\circ}$ $p \leq 0.01$, $^{\circ\circ\circ}$ $p \leq 0.001$.

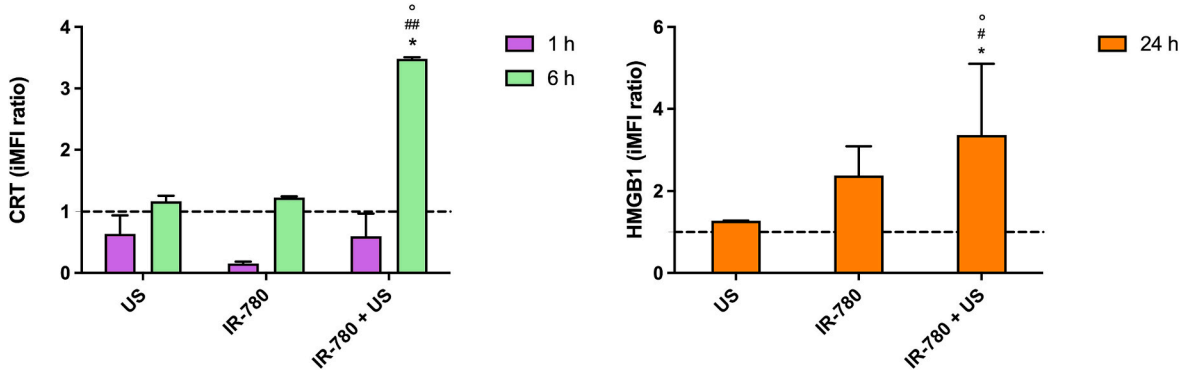

Fig. 3. Evaluation of calreticulin (CRT) and high mobility group box 1 (HMGB1) after sonodynamic therapy (SDT) with IR-780 in two-dimensional BxPC-3 cell cultures. BxPC-3 cells were incubated for 24 h with IR-780 (5 μg/mL) and were then exposed to US (0.63 W/cm^2, 1.505 MHz, continuous wave mode for 3 min). The presence of CRT and HMBG1 was detected 1 and 6 h after the treatment as integrated mean fluorescence intensity (iMFI) ratio and results are expressed as mean ± standard deviation (dashed line representing untreated cells, Ctrl). Statistically significant difference *versus* untreated cells: * $p \leq 0.05$; statistically significant difference between IR-780 + US and IR-780: $^{\#}$ $p \leq 0.05$, and statistically significant difference between IR-780 + US and US: $^{\circ}$ $p \leq 0.05$.

3.4. Dendritic Cell Activation as Induced by SDT with IR-780 in BxPC-3 Cells Co-Cultured with Peripheral Blood Mononuclear Cells

In vitro co-cultures of tumour cells and peripheral blood mononuclear cells (PBMCs) enable the immune system and its response to changes in the tumour microenvironment to be explored [29]. Dendritic cells (DCs) are contained in the PBMC infiltrate from most cancer types and have a protective role in antitumor immunity. Within tumours, infiltrating DCs are heterogeneous in terms of their maturation, differentiation and state of activation, which are controlled and regulated by several microenvironmental signals [30]. CD83 is a member of the immunoglobulin superfamily, and has been identified as being expressed on mature and activated DCs [31]. Therefore, at this stage, our aim was to identify the possible occurrence of activated DCs in the presence of SDT-treated BxPC-3 cells. Possible DC activation was then investigated by co-culturing PBMCs with BxPC-3 cells, which had previously been treated with SDT for 1, 12 and 24 h. Specifically, the DC activation marker (CD83$^+$) was monitored over time by quantifying fluorescence signals for all conditions and by relating them to untreated cells (Ctrl) at each time point (Fig. 4). A significant increase in DC activation in PBMCs (increase in CD83$^+$ cells) in co-culture with SDT-treated BxPC-3 cells was detected after 1 h of co-culturing ($p \leq 0.01$). Furthermore, levels of PBMC activation were similar to those of untreated cells after 12 and 24 h of co-culturing; this maybe due to the allogenic nature of the two different cell lines. Moreover, no significant decrease in tumour cell population (CD326$^+$ cells) was detected at any time point (data not shown).

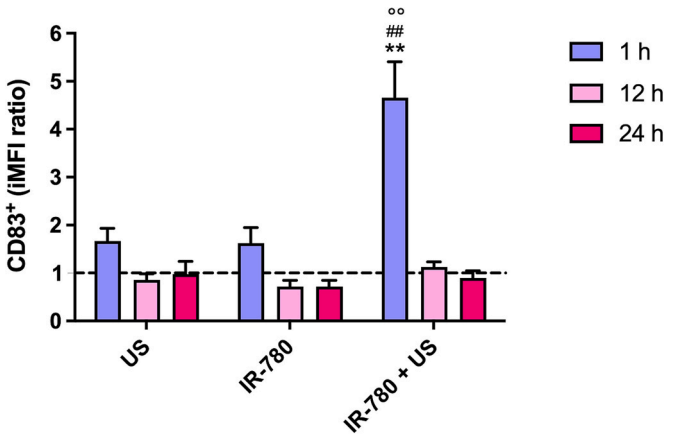

Fig. 4. Evaluation of dendritic cells activation (CD83$^+$ cells). BxPC-3 cells were incubated for 24 h with IR-780 (5 μg/mL) and then exposed to US (0.63 W/cm^2, 1.505 MHz, continuous wave mode for 3 min). One hour after treatment, BxPC-3 cells were co-cultured with peripheral blood mononuclear cells (PBMCs, 1:1) for 1, 12 and 24 h. The presence of CD83$^+$ cells was detected as mean fluorescence intensity (iMFI) ratio by flow cytometry and results are expressed as mean ± SD (dashed line representing untreated cells, Ctrl). Statistically significant difference between treated cells and Ctrl: ** $p \leq 0.01$; statistically significant difference between IR-780 + US and IR-780: $^{\#\#}$ $p \leq 0.01$ and statistically significant difference between IR-780 + US and US: $^{\circ\circ}$ $p \leq 0.01$.

3.5. IR-780 Uptake in BxPC-3 Spheroids

Since spheroids are characterized by several more layers of cells than the classic distribution in 2D cell cultures [23,32], the internalization of IR-780 by BxPC-3 spheroids was properly determined. For this purpose, flow cytometry and confocal microscopy were performed using higher IR-780 concentrations than those used in 2D cell cultures (Fig. 1B), according to the fluorescent properties of the sonosensitizer. Fig. 5A demonstrates that a statistically significant increase in IR-780 fluorescence was detected in spheroids incubated for 24 h at increasing IR-780 concentrations (20 and 30 μg/mL). However, it is important to underline that a reduction in cell viability was observed (data not shown) when spheroids were incubated with IR-780 at 30 μg/mL. Therefore, an IR-780 concentration of 20 μg/mL was used for further SDT experiments on 3D BxPC-3 structures. IR-780 internalization in BxPC-3 spheroids was also confirmed *via* confocal microscopy investigation (Fig. 5B), where a higher IR-780 fluorescent signal can be observed in the crown of the spheroids and a lower signal in the inner core of the 3D structures.

3.6. Effects of Sonodynamic Treatment on BxPC-3 Spheroids

The use of tissue-engineered 3D models of cancer has grown, in recent years, with advances in the field of cancer research and 3D models, which are a more biomimetic platform than 2D cell monolayers grown on tissue-culture plastic [33]. After observing the considerable effect that IR-780 has on 2D cell cultures under US exposure, it was of interest to investigate SDT activity in 3D cell cultures. BxPC-3 spheroids were incubated at a suitable sonosensitizer concentration (IR-780 20 μg/mL) for 24 h prior to US exposure. This was followed by the acquisition of microscopy imagines to detect possible alterations in spheroidal structure and to ascertain spheroid volumes. Under both conditions sets, US alone and SDT (IR-780 + US), spheroids exhibited slight changes in morphology with the sloughing of outer layers possibly being due US-mediated damage, which was more apparent under the SDT conditions after 24 h (data not shown). To evaluate the possible effects of SDT on spheroid growth, spheroid volume was also measured at 24 and 48 h post-treatment. SDT was able to significantly reduce spheroid volume

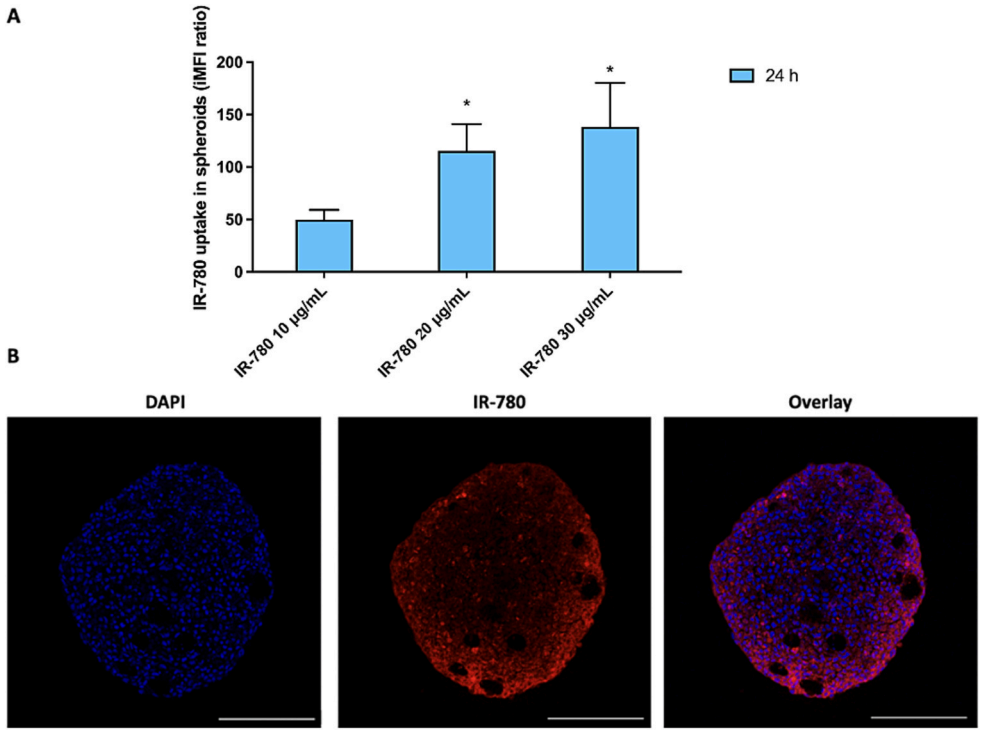

Fig. 5. Uptake of IR-780 by BxPC-3 spheroids. A) BxPC-3 spheroids were incubated with increasing concentrations of IR-780 (10, 20 and 30 µg/mL) for 24 h and the uptake was determined as integrated mean fluorescence intensity (iMFI) ratio by flow cytometry and results are expressed as mean ± standard deviation. Statistically significant difference *versus* untreated spheroids (Ctrl): * $p \leq 0.05$. B) Representative confocal imagines of IR-780 (20 µg/mL) distribution in a BxPC-3 spheroid section. Magnification: 20×. Scale bars: 100 µm.

compared to untreated spheroids ($p \leq 0.05$) and IR-780-treated spheroids ($p \leq 0.05$) 24 h after the treatment, and compared to untreated spheroids ($p \leq 0.01$), IR-780-treated spheroids ($p \leq 0.05$) and US-treated spheroids ($p \leq 0.05$) 48 h after the treatment (Fig. 6).

As investigation into the SDT-mediated effect against BxPC-3 spheroids and analyses of the cell death induced by the treatment are of great interest, spheroids were stained with propidium iodide (PI) and analysed 48 h post-treatment. Fig. 7 shows an increased PI fluorescence in spheroids incubated with IR-780 and subsequently exposed to US,

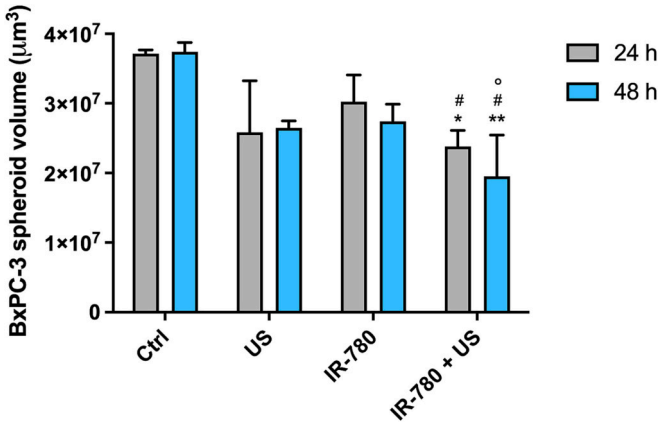

Fig. 6. Effect of sonodynamic therapy with IR-780 on BxPC-3 spheroid volume. BxPC-3 spheroids were incubated with IR-780 (20 µg/mL) for 24 h and then exposed to US (1.66 W/cm^2, 1.505 MHz, 60% duty cycle for 3 min). Spheroid volumes were calculated 24 and 48 h after US exposure and results are expressed as mean ± standard deviation. Statistically significant difference *versus* untreated spheroids (Ctrl): * $p \leq 0.05$, ** $p \leq 0.01$; statistically significant difference between IR-780 + US and IR-780: $^{\#}$ $p \leq 0.05$ and statistically significant difference between IR-780 + US and US: $^{\circ}$ $p \leq 0.05$.

which essentially highlights an increase in dead cells. To support the results obtained in fluorescence analysis, PI fluorescence intensity was also evaluated, and a significant increase in PI intensity was observed in the spheroids treated with SDT ($p \leq 0.01$), compared to the untreated spheroids (Fig. 7). Furthermore, these data were confirmed by an assay used to discriminate live from dead cells in spheroid sections (for detailed information, see the Supporting Information), where an increased PI signal was observed up to the core of spheroids, treated with IR-780 and US, has been observed (Fig. S4), along with a disorganization of spheroid compactness.

3.7. Induction of Immunogenic Cell Death-Related Damage Associated Molecular Patterns by SDT on BxPC-3 Spheroids

To gain insights into the therapeutic potential of SDT, it is imperative to explore the SDT-mediated ICD in a 3D model. As far as we know, this experiment represents the first immunofluorescence investigation of ICD-related DAMPs directly on spheroid sections. Fig. 8A displays the homogenous distribution of the CRT signal in the untreated, US alone and IR-780 alone conditions. Forty-eight hours post-SDT-mediated treatment (IR-780 + US), the translocation of CRT clusters can be observed into several parts of the spheroid section. At the same time, HMGB1 also showed a different fluorescence pattern upon treatment with SDT, with this pattern being slightly different to those observed in the untreated, US alone and IR-780 alone treatment conditions (Fig. 8B).

4. Discussion

Pancreatic cancer is the third leading cause of cancer-related deaths worldwide and is showing increased incidence [34]. Pancreatic ductal adenocarcinoma (PDAC) represents 90% of all pancreatic tumours and is considered one of the most difficult to treat, with a five-year survival rate of <10% [35]. The only potentially curative treatment is represented by surgical resection, however only a limited number of patients

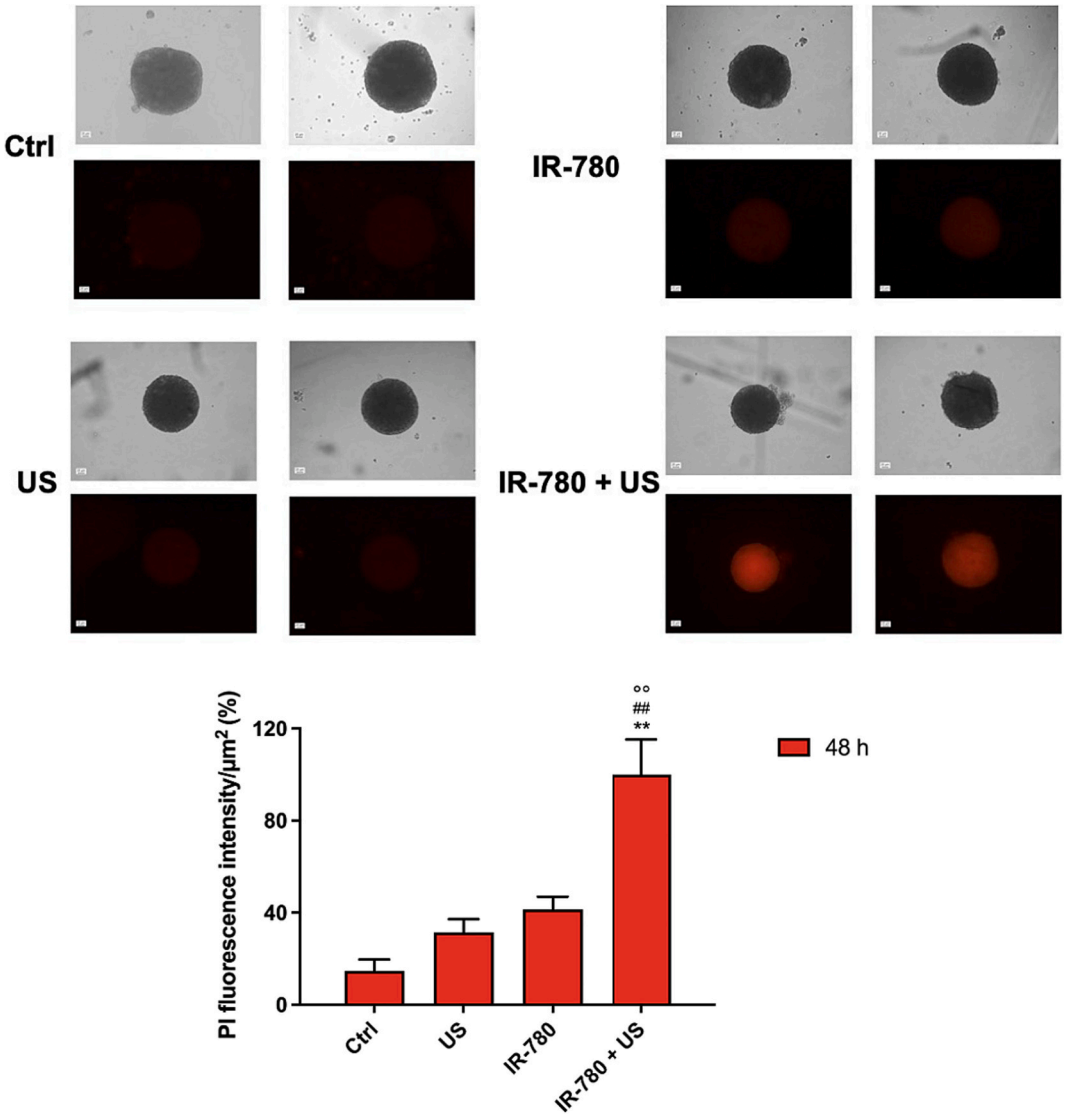

Fig. 7. Fluorescence images of BxPC-3 spheroids after sonodynamic therapy (SDT). BxPC-3 spheroids were incubated with IR-780 (20 μg/mL) for 24 h and then exposed to US (1.66 W/cm^2, 1.505 MHz, 60% duty cycle for 3 min). After 24 h, spheroids were stained with propidium iodide (PI, 100 μg/mL). Magnification: 10×. Scale bars: 25 μm. PI fluorescence was also calculated, and results are expressed as the mean of percentage of PI intensity/μm^2 ± standard deviation. Statistically significant difference *versus* untreated spheroids (Ctrl): ** $p \leq 0.01$; statistically significant difference between IR-780 + US and IR-780: °° $p \leq 0.01$; statistically significant between IR-780 + US and US: °° $p \leq 0.01$.

are eligible due to the advanced stage of disease upon diagnosis [36]. Despite chemotherapy's place as a mainstay therapeutic option for PDAC in increasing survival and palliating cancer-related symptoms [35], therapeutic resistance remains a persistent challenge. A deep understanding of the mechanisms of therapeutic resistance and an exploration of new therapeutic approaches are therefore essential [35].

Sonodynamic therapy (SDT) possesses the feature of non-invasiveness, while presenting limited side-effects and the potential for improved therapeutic outcomes in clinical cancer treatment, compared to traditional chemotherapy and radiotherapy. SDT is a stimulus-responsive approach for the treatment of solid tumours and is based on the use of a relatively harmless chemical agent, called a sonosensitizer, which becomes cytotoxic only upon the application of low-intensity ultrasound (US) [37]. The synergic activity of a sonosensitizer and US culminates in ROS-mediated cytotoxicity, whilst avoiding damage to adjacent healthy tissue. The discovery and development of novel sonosensitizers has attracted wide-spread attention as it is one of the most essential factors for successful SDT outcomes [22,38–41]. For instance, IR-780 dye has been investigated as a sonosensitizer agent that results in effective tumour treatment with minimal side effects [42]. Li and colleagues have investigated IR-780 for use as a SDT sensitizer in breast cancer treatment, and demonstrated its remarkable toxicity against 4 T1 breast cancer *in vitro* after 24 h, at various IR-780 concentrations. After being internalized by tumour cells, thanks to the function of the organic anion transporting polypeptide 1B3 (OATP1B3) [43–45]. IR-780 absorbs US energy and becomes activated from a ground-state into an excited state. After returning to the ground-state, the released energy can generate singlet molecular oxygen and hydrogen peroxide, which can cause tumour cell apoptosis and necrosis [22].

In agreement with these results, the aim of this work is that of exploring US efficacy in activating IR-780 in two-dimensional (2D) and three-dimensional (3D) models of human pancreatic cancer. Furthermore, the feasibility of SDT as a trigger for immunogenic cell death (ICD), thus promoting antitumor immunity, has been specifically evaluated.

Considering the capacity of BxPC-3 cells to internalize IR-780 after 24 h of incubation, SDT effectiveness in reducing cell proliferation was

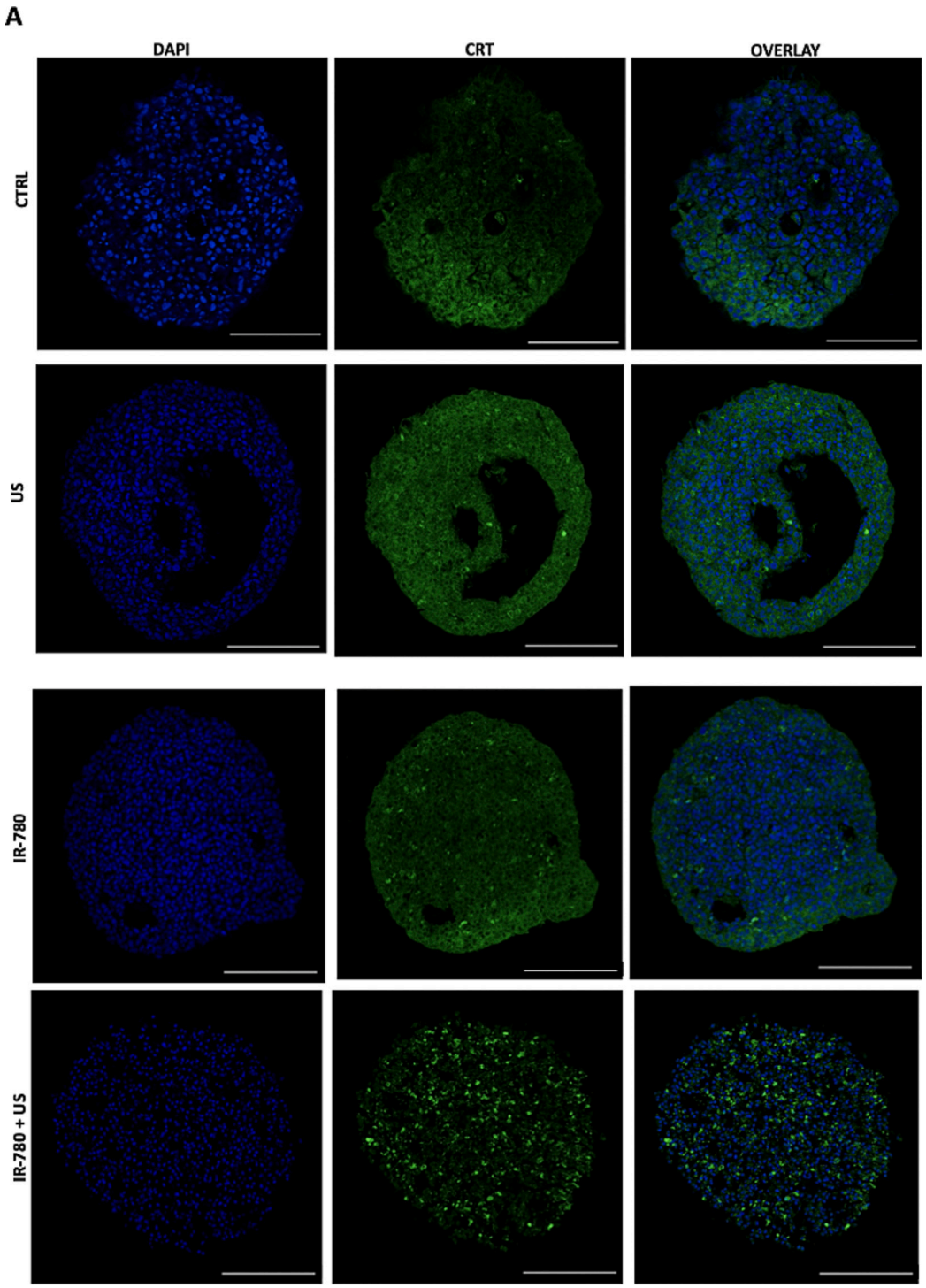

Fig. 8. Representative confocal images of BxPC-3 spheroids after sonodynamic therapy. BxPC-3 spheroids were incubated with IR-780 (20 μg/mL) and then exposed to US (1.66 W/cm^2, 1.505 MHz, 60% duty cycle for 3 min). After 48 h, spheroids labelled with calreticulin (CRT) antibody (panel A) and the high mobility group box 1 (HMGB1) antibody (panel B) were analysed *via* confocal acquisition. Magnification: 20×. Scale bars: 100 μm.

determined at 24, 48 and 72 h, with a significant reduction in cell proliferation being observed 72 h after SDT with a non-cytotoxic concentration of IR-780 5 μg/mL, thus suggesting that a synergistic effect between US and the sonosensitizer is at work. These data are also supported by the identification of a significant increase in late apoptotic cells along with a significant reduction in live cells 48 h after treatment.

The SDT mechanism of action is still under debate and different mechanisms have been suggested: i) sonomechanical effects leading to membrane disruption; ii) sonochemical effects leading to lipid peroxidation; and iii) sonoluminescence leading to ROS generation [16]. In our opinion, the pivotal SDT mechanism is based on the occurrence of acoustic cavitation-induced sonoluminescence, subsequent sonosensitizer activation and reactive oxygen species (ROS) production [46]. The exposure of IR-780 to US in BxPC-3 cells led to significant ROS production, as was also highlighted in breast cancer cells by Li et al. [22]. Moreover, several studies have identified that not only can ROS directly

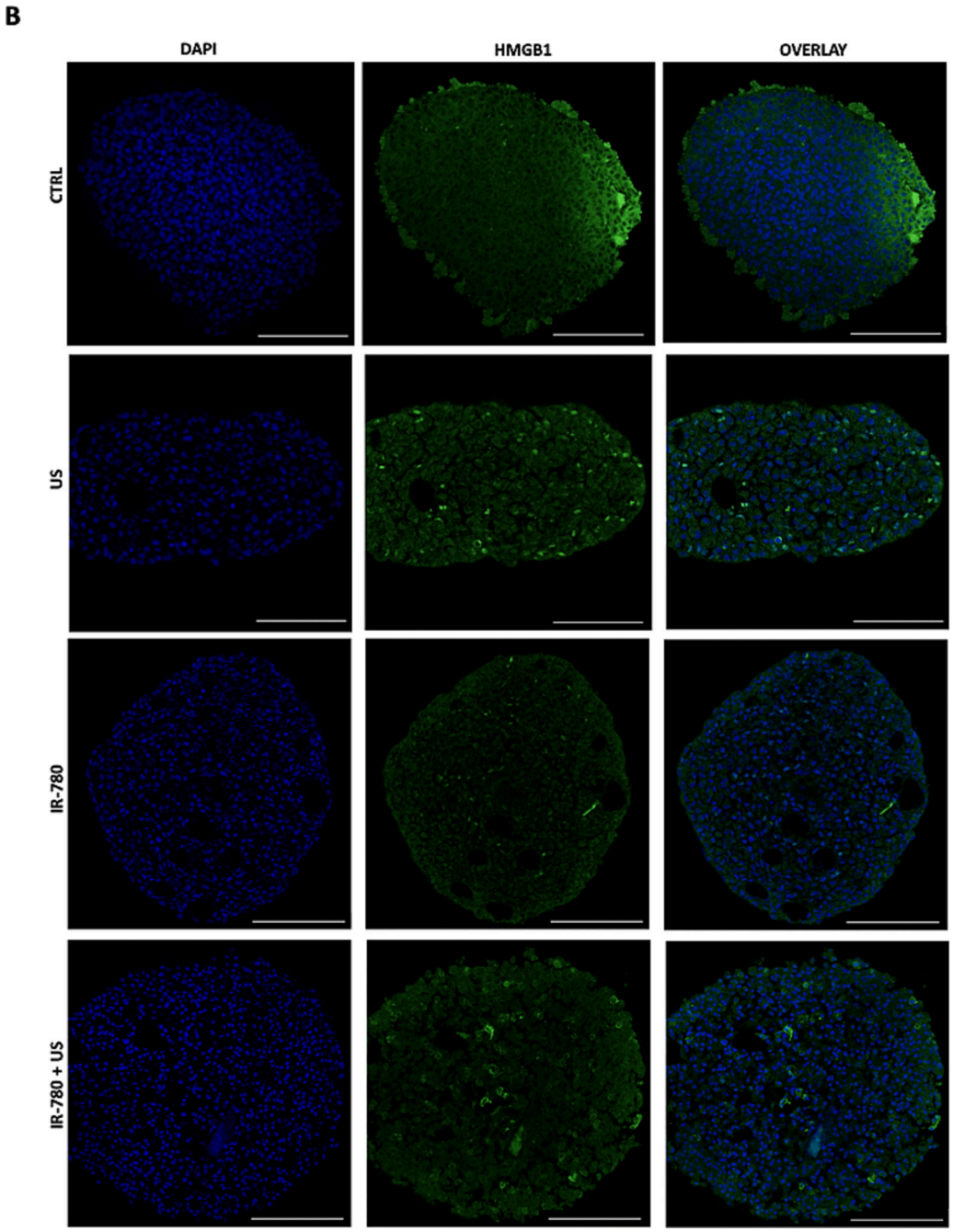

Fig. 8. (*continued*).

kill cancer cells, but that ROS may also be responsible for the induction of ICD and the related release of tumour-associated antigens and damage associated molecular patterns (DAMPs), which strengthens local tumour immunogenicity [47]. In this way, dying cancer cells, which can act as a tumour vaccine, induce a tumour-specific immune response that can target live cancer cells and residual tumour tissue [48]. Indeed, ICD leads to the release of DAMPs, which can activate a specific immune response, from dying cell [27]. This immune response resembles something similar to immunotherapy, which, at present, is a promising therapeutic strategy for cancer treatment as its goal is to generate a robust immune response to eradicate tumour cells and ultimately achieve long-term anticancer immunity [49].

Zhang and colleagues [42] have investigated a therapeutic strategy to assess whether SDT can induce ICD, in association with the sonosensitizer HiPorfin, in a human liver cancer cell line. Calreticulin (CRT) is a distinct DAMP that can be observed on the surface of cells undergoing ICD, and, in fact, the authors detected significant CRT expression after SDT, indicating that SDT can, indeed, induce ICD. Their results also showed that SDT promotes the secretion of pro-inflammatory cytokines (like IFN-γ and IL-2) and the switch from Th2 to Th1 cells, which activate the immune system to elicit anticancer effects, in tumours [42]. An additional study conducted within our research group identified that CRT exposure and the presence of high mobility group box 1 (HMGB1), a late ICD inducer, can be caused by the US stimulation of hypericin in the human HT-29 colon cancer cell line [50].

Taking these results into consideration, we can state that IR-780-mediated SDT treatment against BxPC-3 cells triggers a significant increase in cell surface exposure of CRT after 6 h and HMGB1 after 48 h. This suggests that the US-mediated activation of IR-780 can not only lead to a synergistic anticancer effect but also to ICD. The induction of

ICD can stimulate dying cancer cells to enhance anticancer immunity through the maturation of dendritic cells and the activation of cytotoxic T lymphocytes, as well as by increasing the cytotoxic function of NK cells [27]. Specifically, DC maturation is triggered by DAMPs and allows DCs to migrate from peripheral tissues to secondary lymphoid organs, where the antigen presentation of activating T lymphocytes may take place. The interaction between antigen-specific T cells and mature DCs represents the elicitation of antigen-specific immune responses [51]. Wang and colleagues have reported that the use of 5-aminolevulinic acid, in combination with low-intensity US, suppresses the proliferation, adhesion and migration of murine melanoma B16F10 cells. They showed that the expression levels of the markers for DC maturation, CD68 and CD80, were significantly higher in mice treated with SDT than those in the control group, suggesting that SDT may promote the maturation of DCs, and thus enhance anti-tumour immunity [52].

In vitro experimental models, such as co-cultures between tumour cells and peripheral blood mononuclear cells (PBMCs) that include lymphocytes, monocytes, NK cells and DCs, are therefore useful methods with which to characterize tumour-immune system interplay. Doumba and colleagues performed an *in vitro* co-culture model to study cell-to-cell interactions between primary hepatocellular carcinoma cancer cells (HCC) and autologous PBMCs; they observed that this direct interaction leads to increased antigen-presenting ability of HCC, PBMC activation and the subsequent apoptosis of activated $CD8^+$ T cells [53].

To further investigate whether our sonodynamic approach is able to promote ICD and subsequent DC activation, the effect of co-culturing PBMCs with BxPC-3 cells that had previously been exposed to SDT was explored at different time points (1, 12 and 24 h), according to the timing of DAMP exposure. Indeed, CRT favours the uptake of dying tumour cells by DCs, while HMGB1 can be sensed by DCs through Toll-like receptor 4, thereby promoting the efficient processing and cross-presentation of tumour-associated antigens derived from dying cancer cells [54]. Recent studies have focused on CD83 as a potential target for therapeutic intervention, since high-density CD83 expression is considered a marker for human DC maturation; it has been reported that high levels of surface CD83 have been expressed by freshly isolated blood DCs within 6 h of *in vitro* culture [55].

After co-culturing PBMCs with BxPC-3 cells, for 1, 12, 24 h, a small percentage of mature $CD83^+$ DCs was detected in untreated tumour cells, with this probably being due to the heterologous nature of tumour cells and PBMCs. Interestingly, under the co-culture conditions in which BxPC-3 cells had previously been treated with IR-780 + US, a significant increase in $CD83^+$ DCs, compared to results in the co-culture between PBMCs and untreated tumour cells, was observed after 1 h. This increase was calculated by considering the normalized iMFI values relative to the corresponding untreated conditions. In terms of tumour cell population, BxPC-3 $CD326^+$ cells were detected at each time point, and no significant reduction in their cellular percentage was observed in the PBMC co-culture. These findings are consistent with the results of IR-780 cytotoxicity under US exposure, which demonstrated a significant effect on tumour cells as early as 24 h post-treatment.

The results obtained from 2D cell cultures provided a foundation for investigating the effects of SDT on 3D cell cultures. In recent years, an increasing number of techniques have been developed to facilitate the growth of spheroids *in vitro*, as these models closely resemble the structure and functionality of physiological tissues [23]. Spheroids exhibit tissue-like architecture and exhibit limited drug penetration through tissue, since drugs are mainly confined to the outer cell layers. Spheroids are therefore a better model for drug evaluation compared to classic monolayer cultures [56]. To assess the cellular uptake of IR-780 in spheroids, different concentrations of IR-780 were initially examined, followed by a confocal evaluation of IR-780 distribution within spheroid sections. The confocal analysis, revealed the presence of IR-780 within the inner regions of the spheroidal structure, suggesting that the sonosensitizer was able to deeply penetrate the spheroidal structure.

Based on this knowledge, BxPC-3 spheroids were incubated with IR-780 at a concentration of 20 μg/mL and treated with US after 24 h. Remarkably, a significant reduction in the volume of SDT-treated spheroids, compared to the volume of untreated spheroids, was observed. This reduction in volume was further confirmed in a cell death analysis using PI staining 48 h after treatment; an increase in the number of dead cells was noted. Recent studies have highlighted the relevance of investigating US as a triggering agent for sonosensitizers in specific target sites within 3D models. This approach offers the advantage of easily regulating the physical parameters of US [57,58]. In our study, it was necessary to modify US intensity and the insonation mode when transitioning from 2D to 3D cell cultures in order to achieve a sonodynamic anticancer effect. This adjustment was necessary to ensure optimal US energy release in a way that was tailored to the geometry of the target area.

To further investigate the effect of SDT on 3D structures, an evaluation of ICD was conducted BxPC-3 spheroids. To the best of our knowledge, our data are the first attempt to demonstrate ICD induction within the inner layers of 3D cell cultures. This novel approach allows us to highlight the connection between SDT and ICD in more complex structures compared to classic monolayer cell cultures. Under SDT conditions, we visually observed the presence of CRT in spheroid sections. Compared to the control group, single spots of CRT were clearly visible, whilst the treated and untreated conditions led to an evident, but slight, difference in HMGB1 occurrence. These data highlight a variation in the signalling of ICD-related DAMPs in 3D sections, compared to data obtained from 2D models. This disparity may be influenced by the different time points used to detect CRT in the 2D and 3D models. Therefore, in 3D models, where the cellular architecture is more complex than 2D cell culture, we can hypothesize that the CRT signal finds a richer microenvironment within which to propagate across cell layers, allowing it to persist for longer. This ICD-related DAMP, therefore, serves as both a primitive pro-phagocytic signalling protein and an a "eat-me" signal for immune cell recognition, as emphasized by Zhang [59].

5. Conclusions

The exposure of IR-780 to ultrasound (US) successfully provoked a significant anticancer effect by triggering the sonosensitizer cytotoxicity as well as inducing immunogenic cell death (ICD) induction not only in two-dimensional (2D), but also in three-dimensional (3D) pancreatic cancer cell cultures. The efficacy of sonodynamic therapy (SDT) with IR-780 on BxPC-3 spheroids confirms the anticancer potential observed in the 2D BxPC-3 model, albeit with notable differences in US parameters. This highlights the importance of investigating *in vitro* 3D cancer models before proceeding to *in vivo* studies. Moreover, SDT's observed lower effect on the growth of 3D cancer cultures, compared to that 2D cancer cultures, indicates that further studies into different treatment schedules that allow for multiple US exposures should be performed. These results also suggest that SDT may be feasibility investigated for use in combination with chemotherapy and immunotherapy, thanks to its intrinsic selectivity, which hinders systemic toxicity.

The evaluation of ICD in 3D BxPC-3 cell cultures highlighted the presence of ICD-related damage associated molecular patterns, mirroring observations in 2D BxPC-3 cell cultures. Additionally, the activation of the immune system was confirmed in co-cultures of SDT-treated BxPC3 cells and peripheral blood mononuclear cells. This type of cell death leads to an adaptive immune response that is specific to antigens derived from dead cells. However, it should be emphasized the need for confirmation of SDT immunomodulatory effect in relevant *in vivo* models. Despite the challenges associated with selecting appropriate US parameters to achieve therapeutic efficacy in SDT, this approach deserves further preclinical studies to enable the decision to engage clinical studies as a promising anticancer strategy, particularly for tumours with low responsiveness to conventional drug treatments. Finally, SDT-induced ICD has the potential to evoke long-lasting protective antitumor

immunity that may combat the issue of tumour relapse which remains a significant challenge in cancer treatment.

CRediT authorship contribution statement

Federica Foglietta: Investigation, Writing – original draft. **Patrizia Panzanelli:** Methodology. **Riccardo Pizzo:** Formal analysis, Visualization. **Marta Giacone:** Data curation. **Carlo Della Pepa:** Conceptualization, Validation. **Gianni Durando:** Resources. **Loredana Serpe:** Funding acquisition, Project administration, Writing – review & editing. **Roberto Canaparo:** Conceptualization, Supervision.

Funding

This research was funded by the University of Torino (Ricerca Locale 2021 and Ricerca Locale 2022).

Declaration of competing interest

The authors declare that they have no known competing financial interests or personal relationships that could have appeared to influence the work reported in this paper.

Data availability

Data will be made available on request.

Acknowledgments

The authors would like to thank Dr. Sian Farrell for her deep revision of the manuscript.

Appendix A. Supplementary data

Supplementary data to this article can be found online at https://doi.org/10.1016/j.jphotobiol.2024.112842.

References

[1] J. Ushio, A. Kanno, E. Ikeda, K. Ando, H. Nagai, T. Miwata, Y. Kawasaki, Y. Tada, K. Yokoyama, N. Numao, K. Tamada, A.K. Lefor, H. Yamamoto, Pancreatic ductal adenocarcinoma: epidemiology and risk factors, Diagnostics. 11 (2021) 562, https://doi.org/10.3390/diagnostics11030562.
[2] R.L. Siegel, K.D. Miller, N.S. Wagle, A. Jemal, Cancer statistics, 2023, CA Cancer J. Clin. 73 (2023) 17–48, https://doi.org/10.3322/caac.21763.
[3] O. Partyka, M. Pajewska, D. Kwaśniewska, A. Czerw, A. Deptała, M. Budzik, E. Cipora, I. Gąska, L. Gazdowicz, A. Mielnik, K. Sygit, M. Sygit, E. Krzych-Fałta, D. Schneider-Matyka, S. Grochans, A.M. Cybulska, J. Drobnik, E. Bandurska, W. Ciećko, P. Ratajczak, K. Kamecka, M. Marczak, R. Kozłowski, Overview of pancreatic Cancer epidemiology in Europe and recommendations for screening in high-risk populations, Cancers (Basel). 15 (2023) 3634, https://doi.org/10.3390/cancers15143634.
[4] E. van Veldhuisen, C. van den Oord, L.J. Brada, M.S. Walma, J.A. Vogel, J. W. Wilmink, M. del Chiaro, K.P. van Lienden, M.R. Meijerink, G. van Tienhoven, T. Hackert, C.L. Wolfgang, H. van Santvoort, B. Groot Koerkamp, O.R. Busch, I. Q. Molenaar, C.H. van Eijck, M.G. Besselink, Locally Advanced Pancreatic Cancer: Work-Up, Staging, and Local Intervention Strategies, Cancers (Basel) vol. 11, 2019, p. 976, https://doi.org/10.3390/cancers11070976.
[5] G.M. O'Kane, F. Ladak, S. Gallinger, Advances in the management of pancreatic ductal adenocarcinoma, Can. Med. Assoc. J. 193 (2021) E844–E851, https://doi.org/10.1503/cmaj.201450.
[6] Z. Szondy, Z. Sarang, B. Kiss, É. Garabuczi, K. Köröskényi, Anti-inflammatory mechanisms triggered by apoptotic cells during their clearance, Front. Immunol. 8 (2017), https://doi.org/10.3389/fimmu.2017.00909.
[7] G. Kroemer, L. Galluzzi, O. Kepp, L. Zitvogel, Immunogenic cell death in Cancer therapy, Annu. Rev. Immunol. 31 (2013) 51–72, https://doi.org/10.1146/annurev-immunol-032712-100008.
[8] G. Kroemer, C. Galassi, L. Zitvogel, L. Galluzzi, Immunogenic cell stress and death, Nat. Immunol. 23 (2022) 487–500, https://doi.org/10.1038/s41590-022-01132-2.
[9] A.D. Garg, A.M. Dudek-Peric, E. Romano, P. Agostinis, Immunogenic cell death, Int. J. Dev. Biol. 59 (2015) 131–140, https://doi.org/10.1387/ijdb.150061pa.
[10] A.D. Garg, P. Agostinis, ER stress, autophagy and immunogenic cell death in photodynamic therapy-induced anti-cancer immune responses, Photochem. Photobiol. Sci. 13 (2014) 474–487, https://doi.org/10.1039/c3pp50333j.
[11] M. Kielbik, I. Szulc-Kielbik, M. Klink, Calreticulin—multifunctional chaperone in immunogenic cell death: potential significance as a prognostic biomarker in ovarian Cancer patients, Cells. 10 (2021) 130, https://doi.org/10.3390/cells10010130.
[12] J. Lou, M. Aragaki, N. Bernards, T. Chee, A. Gregor, Y. Hiraishi, T. Ishiwata, C. Leung, L. Ding, S. Kitazawa, T. Koga, Y. Sata, H. Ogawa, J. Chen, T. Kato, K. Yasufuku, G. Zheng, Repeated photodynamic therapy mediates the abscopal effect through multiple innate and adaptive immune responses with and without immune checkpoint therapy, Biomaterials. 292 (2023) 121918, https://doi.org/10.1016/j.biomaterials.2022.121918.
[13] A. Sofuni, T. Itoi, Current status and future perspective of sonodynamic therapy for cancer, J. Med. Ultrason. (2022), https://doi.org/10.1007/s10396-022-01263-x.
[14] H. Chen, L. Liu, A. Ma, T. Yin, Z. Chen, R. Liang, Y. Qiu, M. Zheng, L. Cai, Noninvasively immunogenic sonodynamic therapy with manganese protoporphyrin liposomes against triple-negative breast cancer, Biomaterials. 269 (2021) 120639, https://doi.org/10.1016/j.biomaterials.2020.120639.
[15] L. Dong, W. Li, L. Sun, L. Yu, Y. Chen, G. Hong, Energy-converting biomaterials for cancer therapy: category, efficiency, and biosafety, WIREs Nanomedicine and Nanobiotechnology. 13 (2021), https://doi.org/10.1002/wnan.1663.
[16] R. Canaparo, F. Foglietta, N. Barbero, L. Serpe, The promising interplay between sonodynamic therapy and nanomedicine, Adv. Drug Deliv. Rev. 189 (2022) 114495, https://doi.org/10.1016/j.addr.2022.114495.
[17] W. Lopez, N. Nguyen, J. Cao, C. Eddow, K.K. Shung, N.S. Lee, M.S.S. Chow, Ultrasound therapy, chemotherapy and their combination for prostate Cancer, Technol. Cancer Res. Treat. 20 (2021), https://doi.org/10.1177/15330338211011965, 153303382110119.
[18] F. Foglietta, V. Pinnelli, F. Giuntini, N. Barbero, P. Panzanelli, G. Durando, E. Terreno, L. Serpe, R. Canaparo, Sonodynamic treatment induces selective killing of Cancer cells in an in vitro co-culture model, Cancers (Basel). 13 (2021) 3852, https://doi.org/10.3390/cancers13153852.
[19] N. Wu, C.-H. Fan, C.-K. Yeh, Ultrasound-activated nanomaterials for sonodynamic cancer theranostics, Drug Discov. Today 27 (2022) 1590–1603, https://doi.org/10.1016/j.drudis.2022.02.025.
[20] Z. He, S. Zhang, Tumor-associated macrophages and their functional transformation in the hypoxic tumor microenvironment, Front. Immunol. 12 (2021), https://doi.org/10.3389/fimmu.2021.741305.
[21] S. Chen, J. Wang, H. Liao, K. Tang, Y. Xu, L. Wang, C. Niu, M1 macrophage-derived Sonoresponsive nanoparticles for Sonodynamic anticancer therapy, Int. J. Nanomedicine 17 (2022) 4725–4741, https://doi.org/10.2147/IJN.S381170.
[22] Y. Li, Q. Zhou, Z. Deng, M. Pan, X. Liu, J. Wu, F. Yan, H. Zheng, IR-780 dye as a Sonosensitizer for Sonodynamic therapy of breast tumor, Sci. Rep. 6 (2016) 25968, https://doi.org/10.1038/srep25968.
[23] F. Foglietta, R. Canaparo, G. Muccioli, E. Terreno, L. Serpe, Methodological aspects and pharmacological applications of three-dimensional cancer cell cultures and organoids, Life Sci. 254 (2020) 117784, https://doi.org/10.1016/j.lfs.2020.117784.
[24] T. Franchi-Mendes, R. Eduardo, G. Domenici, C. Brito, 3D Cancer models: depicting cellular crosstalk within the tumour microenvironment, Cancers (Basel). 13 (2021) 4610, https://doi.org/10.3390/cancers13184610.
[25] L. Serpe, R. Canaparo, G. Varchi, M. Ballestri, F. Federica Foglietta, G. Sotgiu, A. Guerrini, A. Francovich, P. Civera, R. Frairia, Polymeric nanoparticles enhance the sonodynamic activity of meso-tetrakis (4-sulfonatophenyl) porphyrin in an in vitro neuroblastoma model, Int. J. Nanomedicine (2013) 4247, https://doi.org/10.2147/IJN.S51070.
[26] F. Giuntini, F. Foglietta, A.M. Marucco, A. Troia, N.V. Dezhkunov, A. Pozzoli, G. Durando, I. Fenoglio, L. Serpe, R. Canaparo, Insight into ultrasound-mediated reactive oxygen species generation by various metal-porphyrin complexes, Free Radic. Biol. Med. 121 (2018) 190–201, https://doi.org/10.1016/j.freeradbiomed.2018.05.002.
[27] Z. Asadzadeh, E. Safarzadeh, S. Safaei, A. Baradaran, A. Mohammadi, K. Hajiasgharzadeh, A. Derakhshani, A. Argentiero, N. Silvestris, B. Baradaran, Current approaches for combination therapy of Cancer: the role of immunogenic cell death, Cancers (Basel). 12 (2020) 1047, https://doi.org/10.3390/cancers12041047.
[28] S.T. Workenhe, J. Pol, G. Kroemer, Tumor-intrinsic determinants of immunogenic cell death modalities, Oncoimmunology. 10 (2021), https://doi.org/10.1080/2162402X.2021.1893466.
[29] G. Borsci, S. Barbieri, I. Guardamagna, L. Lonati, A. Ottolenghi, G.B. Ivaldi, M. Liotta, P. Tabarelli de Fatis, G. Baiocco, M. Savio, Immunophenotyping reveals no significant perturbation to PBMC subsets when co-cultured with colorectal adenocarcinoma Caco-2 cells exposed to X-rays, Front. Immunol. 11 (2020), https://doi.org/10.3389/fimmu.2020.01077.
[30] M.B. Giorello, A. Matas, P. Marenco, K.M. Davies, F.R. Borzone, M.L. Calcagno, H. García-Rivello, A. Wernicke, L.M. Martinez, V. Labovsky, N.A. Chasseing, CD1a- and CD83-positive dendritic cells as prognostic markers of metastasis development in early breast cancer patients, Breast Cancer 28 (2021) 1328–1339, https://doi.org/10.1007/s12282-021-01270-9.
[31] Z. Li, X. Ju, P.A. Silveira, E. Abadir, W.H. Hsu, D.N.J. Hart, G.J. Clark, CD83: activation marker for antigen presenting cells and its therapeutic potential, Front. Immunol. 10 (2019), https://doi.org/10.3389/fimmu.2019.01312.
[32] K. Białkowska, P. Komorowski, M. Bryszewska, K. Miłowska, Spheroids as a type of three-dimensional cell cultures-examples of methods of preparation and the Most important application, Int. J. Mol. Sci. 21 (2020) 6225, https://doi.org/10.3390/ijms21176225.

[33] J. Pape, M. Emberton, U. Cheema, 3D Cancer models: the need for a complex stroma, compartmentalization and stiffness, Front. Bioeng. Biotechnol. 9 (2021), https://doi.org/10.3389/fbioe.2021.660502.
[34] N. Khalaf, H.B. El-Serag, H.R. Abrams, A.P. Thrift, Burden of pancreatic Cancer: from epidemiology to practice, Clin. Gastroenterol. Hepatol. 19 (2021) 876–884, https://doi.org/10.1016/j.cgh.2020.02.054.
[35] V. Tonini, M. Zanni, Pancreatic cancer in 2021: What you need to know to win, World J. Gastroenterol. 27 (2021) 5851–5889. Doi: https://doi.org/10.3748/wjg.v27.i35.5851.
[36] D. Ansari, B. Tingstedt, B. Andersson, F. Holmquist, C. Sturesson, C. Williamsson, A. Sasor, D. Borg, M. Bauden, R. Andersson, Pancreatic cancer: yesterday, today and tomorrow, Future Oncol. 12 (2016) 1929–1946, https://doi.org/10.2217/fon-2016-0010.
[37] Y. Araújo Martins, T. Zeferino Pavan, R. Fonseca Vianna Lopez, Sonodynamic therapy: ultrasound parameters and in vitro experimental configurations, Int. J. Pharm. 610 (2021) 121243, https://doi.org/10.1016/j.ijpharm.2021.121243.
[38] Q.L. Guo, X.L. Dai, M.Y. Yin, H.W. Cheng, H.S. Qian, H. Wang, D.M. Zhu, X. W. Wang, Nanosensitizers for sonodynamic therapy for glioblastoma multiforme: current progress and future perspectives, Mil. Med. Res. 9 (2022) 26, 1186/s40779-022-00386-z.
[39] Y. Yang, X. Wang, H. Qian, L. Cheng, Titanium-based sonosensitizers for sonodynamic cancer therapy, Appl. Mater. Today 25 (2021) 101215, https://doi.org/10.1016/j.apmt.2021.101215.
[40] S. Ning, X. Dai, W. Tang, Q. Guo, M. Lyu, D. Zhu, W. Zhang, H. Qian, X. Yao, X. Wang, Cancer cell membrane-coated C-TiO_2 hollow nanoshells for combined sonodynamic and hypoxia-activated chemotherapy, Acta Biomater. 152 (2022) 562–574, https://doi.org/10.1016/j.actbio.2022.08.067.
[41] L. Sun, X. Wang, F. Gong, K. Yin, W. Zhu, N. Yang, S. Bai, F. Liao, M. Shao, L. Cheng, Silicon nanowires decorated with platinum nanoparticles were applied for photothermal-enhanced sonodynamic therapy, Theranostics. 11 (2021) 9234–9242, https://doi.org/10.7150/thno.58755.
[42] C. Zhang, L. Long, C. Shi, Mitochondria-targeting IR-780 dye and its derivatives: synthesis, mechanisms of action, and Theranostic applications, Adv Ther (Weinh). 1 (2018) 1800069, https://doi.org/10.1002/adtp.201800069.
[43] X. Yi, F. Yan, F. Wang, W. Qin, G. Wu, X. Yang, C. Shao, L.W.K. Chung, J. Yuan, IR-780 dye for near-infrared fluorescence imaging in prostate cancer, Sci Monit. 21 (2015) 511–517, https://doi.org/10.12659/MSM.892437.
[44] V. Buxhofer-Ausch, L. Secky, K. Wlcek, M. Svoboda, V. Kounnis, E. Briasoulis, A. G. Tzakos, W. Jaeger, T. Thalhammer, Tumor-specific expression of organic anion-transporting polypeptides: transporters as novel targets for cancer therapy, J Drug Deliv. 2013 (2013) 863539, https://doi.org/10.1155/2013/863539.
[45] T. Nakanishi, I. Tamai, Putative roles of organic anion transporting polypeptides (OATPs) in cell survival and progression of human cancers, Biopharm. Drug Dispos. 35 (2014) 463–484, https://doi.org/10.1002/bdd.1915.
[46] X. Liu, X. Pan, C. Wang, H. Liu, Modulation of reactive oxygen species to enhance sonodynamic therapy, Particuology. 75 (2023) 199–216, https://doi.org/10.1016/j.partic.2022.08.001.
[47] W. Wu, M. Xu, B. Qiao, T. Huang, H. Guo, N. Zhang, L. Zhou, M. Li, Y. Tan, M. Zhang, X. Xie, X. Shuai, C. Zhang, Nanodroplet-enhanced sonodynamic therapy potentiates immune checkpoint blockade for systemic suppression of triple-negative breast cancer, Acta Biomater. 158 (2023) 547–559, https://doi.org/10.1016/j.actbio.2022.12.023.
[48] J. Zhou, G. Wang, Y. Chen, H. Wang, Y. Hua, Z. Cai, Immunogenic cell death in cancer therapy: present and emerging inducers, J. Cell. Mol. Med. 23 (2019) 4854–4865, https://doi.org/10.1111/jcmm.14356.
[49] A. Showalter, A. Limaye, J.L. Oyer, R. Igarashi, C. Kittipatarin, A.J. Copik, A. R. Khaled, Cytokines in immunogenic cell death: applications for cancer immunotherapy, Cytokine. 97 (2017) 123–132, https://doi.org/10.1016/j.cyto.2017.05.024.
[50] F. Foglietta, R. Canaparo, S. Cossari, P. Panzanelli, F. Dosio, L. Serpe, Ultrasound triggers Hypericin activation leading to multifaceted anticancer activity, Pharmaceutics. 14 (2022) 1102, https://doi.org/10.3390/pharmaceutics14051102.
[51] T.A. Patente, M.P. Pinho, A.A. Oliveira, G.C.M. Evangelista, P.C. Bergami-Santos, J. A.M. Barbuto, Human dendritic cells: their heterogeneity and clinical application potential in Cancer immunotherapy, Front. Immunol. 9 (2019), https://doi.org/10.3389/fimmu.2018.03176.
[52] S. Wang, Z. Hu, X. Wang, C. Gu, Z. Gao, W. Cao, J. Zheng, 5-Aminolevulinic acid–mediated Sonodynamic therapy reverses macrophage and dendritic cell passivity in murine melanoma xenografts, Ultrasound Med. Biol. 40 (2014) 2125–2133, https://doi.org/10.1016/j.ultrasmedbio.2014.05.007.
[53] P.P. Doumba, M. Nikolopoulou, I.P. Gomatos, M.M. Konstadoulakis, J. Koskinas, Co-culture of primary human tumor hepatocytes from patients with hepatocellular carcinoma with autologous peripheral blood mononuclear cells: study of their in vitro immunological interactions, BMC Gastroenterol. 13 (2013) 17, https://doi.org/10.1186/1471-230X-13-17.
[54] S.K. Wculek, F.J. Cueto, A.M. Mujal, I. Melero, M.F. Krummel, D. Sancho, Dendritic cells in cancer immunology and immunotherapy, Nat. Rev. Immunol. 20 (2020) 7–24, https://doi.org/10.1038/s41577-019-0210-z.
[55] C.M. Prazma, T.F. Tedder, Dendritic cell CD83: a therapeutic target or innocent bystander? Immunol. Lett. 115 (2008) 1–8, https://doi.org/10.1016/j.imlet.2007.10.001.
[56] F. Perche, V.P. Torchilin, Cancer cell spheroids as a model to evaluate chemotherapy protocols, Cancer Biol. Ther. 13 (2012) 1205–1213, https://doi.org/10.4161/cbt.21353.
[57] F. Foglietta, L. Serpe, R. Canaparo, The effective combination between 3D Cancer models and stimuli-responsive nanoscale drug delivery systems, Cells. 10 (2021) 3295, https://doi.org/10.3390/cells10123295.
[58] K. Logan, F. Foglietta, H. Nesbitt, Y. Sheng, T. McKaig, S. Kamila, J. Gao, N. Nomikou, B. Callan, A.P. McHale, J.F. Callan, Targeted chemo-sonodynamic therapy treatment of breast tumours using ultrasound responsive microbubbles loaded with paclitaxel, doxorubicin and rose Bengal, Eur. J. Pharm. Biopharm. 139 (2019) 224–231, https://doi.org/10.1016/j.ejpb.2019.04.003.
[59] Y. Zhang, R. Thangam, S.-H. You, R.D. Sultonova, A. Venu, J.-J. Min, Y. Hong, Engineering Calreticulin-targeting Monobodies to detect immunogenic cell death in Cancer chemotherapy, Cancers (Basel). 13 (2021) 2801, https://doi.org/10.3390/cancers13112801.